Multilevel Omics-Readouts of *in vitro* Perturbation Studies are Determined by Memory Effects from Subculture

Patricia Bortel[1,2,†], Gerhard Hagn[1,2,†], Lukas Skos[1,2], Andrea Bileck[3], Verena Paulitschke[4], Philipp Paulitschke[5,6], Lion Gleiter[5], Thomas Mohr[1,7], Christopher Gerner[1,3], Samuel M. Meier-Menches[1,3,8,*]

[1] Department of Analytical Chemistry, Faculty of Chemistry, University of Vienna, Waehringer Str. 38, 1090 Vienna, Austria.

[2] Vienna Doctoral School in Chemistry (DoSChem), University of Vienna, Waehringer Str. 42, 1090 Vienna, Austria.

[3] Joint Metabolome Facility, University of Vienna and Medical University of Vienna, Waehringer Str. 38, 1090 Vienna, Austria.

[4] Department of Dermatology, Medical University of Vienna, Waehringer Guertel 18-20, 1090 Vienna, Austria.

[5] PHIO scientific GmbH, Esswurmstraße 16, 81371 Munich, Germany.

[6] Faculty of Physics, Ludwig-Maximilians University of Munich, Geschwister-Scholl-Platz 1, 80539 Munich, Germany.

[7] Center of Cancer Research, Department of Medicine I, Medical University of Vienna and Comprehensive Cancer Center, 1090 Vienna, Austria.

[8] Institute of Inorganic Chemistry, Faculty of Chemistry, University of Vienna, Waehringer Str. 38, 1090 Vienna, Austria.

[†] These authors contributed equally.

Contacts

samuel.meier-menches@univie.ac.at

Keywords

Arsenic trioxide, Eicosadomics, Mode of action deconvolution, Multilevel omics, Perturbation network, Phosphoproteomics, Proteomics, Reproducibility, Subculture

Abstract

Mass spectrometry-based omics technologies are of increasing relevance for drug discovery. The identification of significant molecular events is a prerequisite in order to map treatments effects to biological pathways for mode of action (MoA) deconvolution. The main contributors to statistical significance are the effect size and the variation of a given molecule. While the former is largely determined by the biological system and the drug treatment, the latter is controlled by the experimental workflow. The impact of sample preparation and instrumentation on variation are well described, but the impact of cell culture conditions on the variation of omics readouts is less explored. Here, we provide evidence that memory effects originating from subculture conditions during cell expansion before the perturbation influence the variation of multilevel omics readouts, including eicosadomics, proteomics and phosphoproteomics, as well as phenotypic parameters, *e.g.* cell growth and motility using a Cellwatcher system. The treatment was carried out in SW480 colon carcinoma cells with the clinically approved anticancer agent arsenic trioxide (ATO), which follows a multi-modal MoA. Experimental variation was assessed using two different subculture conditions. First, the cells were homogeneously expanded in the Log phase before the treatment. Second, the cells were heterogeneously expanded using cells in the Lag, Log and plateau phases of cell growth before the treatment. When comparing the homogeneous and heterogeneous subcultures, the coefficients of variation (CVs) of controls increased from 1% to 3% for eicosadomics, 11% to 23% for proteomics, 24% to 53% for phosphoproteomics, 5% to 13% for growth area occupied and 6% to 14% for cell motility. The ATO treatment did not considerably influence the number of identified molecules by mass spectrometry, nor the fold-change distributions after both subculture conditions. Therefore, the increased number of significant molecular events in drug treatments after homogeneous subculture seems to be mainly caused by the decrease in CVs. This in turn increased the information content in the obtained perturbation network, based on proteomics and phosphoproteomics data, from 58 to 321 causal conjectures after heterogeneous and homogeneous subcultures, respectively. Independently of the subculture conditions, the perturbation networks allowed for delineating the established MoA of ATO, including enhanced kinase signaling and reduced MYC-related gene expression, induction of heat shock proteins and cell cycle disruption. However, only the perturbation network after homogeneous subculture enabled the discovery of unprecedented drug effects, including down-regulation and quadruple dephosphorylation of the transcription factor RB1, among others. Also, the involvement of AP-1, which is central to the MoA of ATO was only detected after homogenous subculture. In summary, memory effects from subculture have broad relevance for MoA testing in drug discovery since they clearly manifest in molecular and phenotypic properties and their control enables a considerably enhanced MoA deconvolution, facilitating discovery efforts.

Introduction

Mass spectrometry (MS)-based omics techniques are increasingly employed to characterize drug-induced perturbations because of their hypothesis-generating power.[1-3] Perturbation studies are enabled by the identification of molecular events that are mapped to biological processes and the resulting perturbation networks aid in deconvoluting drug modes of action (MoA).[1,4,5] Additionally, integrating multilevel omics data allows to infer interaction networks that are not accessible by single omics levels[6-8] and is a powerful tool for causal reasoning.[9,10]

Importantly, the information content of perturbation networks, *i.e.* the number of significant and comprehensible molecular alterations, is determined by experimental and statistical workflows. Omics experiments produce large numbers of variables that are accounted for by stringent significance testing.[11,12] Significance calculations based on p-values consider the effect size and variation of each molecule,[13] which are put into context of all detected molecules during an experiment by multiple testing corrections, *e.g.* false discovery rates (FDRs).[11] While the effect size reports the mean value difference of a molecule that is characteristic for the perturbation of a system,[13] the variation is largely determined by the experimental procedure.[14] Variation is quantified as the relative standard deviation or coefficient of variation (CV) and serves as a key measure for the precision and thus, reproducibility of an experiment or method.[15] Indeed, the reproducibility crisis is a central challenge in omics sciences[16-18] and life sciences in general.[19-23]

Early drug discovery is routinely performed using *in vitro* cell cultures. Perturbation studies are evaluated by the independent analysis of a number of biological replicates of control and drug-treated cells to allow for significance testing.[24,25] In this setup, instrumental MS-based variation is typically low,[16,24,26] while sample preparation methods may have considerable, but predictable effects on experimental variation across omics levels.[27,28] However, the variation induced by biological replicates in one experiment or by the temporal evolution of cell lines during culture may be large and highlights cell culture conditions as a limiting factor for experimental omics readouts.[17,29,30] For example, we evidenced previously that the batch-dependent differences in eicosanoid content of fetal calf serum in the cell culture medium modulates cellular effector functions.[31] Others described that the pH of cell culture medium differentially regulates intracellular pathways across omics layers, including transcriptomics, proteomics and metabolomics.[32] Genetic heterogeneity and instability affects cell phenotypes and drug responses.[30,33] Moreover, cell lines may respond differently to the same perturbation depending on basal expression,[34] cellular plasticity[35] or resistance phenomena, *e.g.* the epithelial-mesenchymal transition.[29,36,37]

Here, we investigate the effects of the anticancer agent arsenic trioxide (ATO)[38,39] on SW480 colon carcinoma cells and demonstrate that subculture conditions directly impact on the variation, but not necessarily on the effect size, or the number of identified molecules of

multilevel omics readouts. These include eicosadomics, proteomics and phosphoproteomics, as well as phenotypic parameters, *e.g.* cell growth and motility, which were monitored in real-time using a Cellwatcher system. Subculture describes the process of transferring cells from one culture flask to another and is generally used to expand cell lines.[40] These subculture phenomena are distinct from confluence-dependent treatment effects[41,42] or phenotypic switches caused by genetic instability after long-term culture.[30,33] In this study, the cells are treated at equal cell numbers with a short perturbation after specified subculture conditions. The influence of these conditions on multilevel omics readouts therefore reflects memory effects from subculture, whose control facilitates the identification of significant molecular events and results in perturbation networks with an enhanced information density that in turn enable a detailed drug MoA deconvolution.

Materials and Methods

Cell Culture

Culture conditions. The colon carcinoma cell line SW480 was kindly provided by Michael Jakupec (Department of Inorganic Chemistry, University of Vienna, Austria). SW480 cells were cultured in Eagle's minimum essential medium (EMEM; Sigma–Aldrich, USA) supplemented with 10% FCS, 1% penicillin/streptomycin, 2 mM L-Glutamine, 0.1 mM non-essential amino acids and 1 mM sodium pyruvate (all Gibco, USA). The cells were grown in a humidified atmosphere with 5% CO_2 at 37°C.

Treatment. SW480 cancer cells were cultured in T75 flasks for adherent cell culture (Sarstedt GmbH, Nümbrecht, Germany). Prior to the drug treatment, three distinct subculture conditions were generated containing cells in different growth phases, including Lag phase (20% growth area occupied, 1 : 20 split), Log phase (75% growth area occupied, 1 : 10 split) and plateau phase (>95% growth area occupied, 1 : 2 split; Supplementary Information, Figure 1). From those T75 flasks, equal numbers of cells were transferred to 6-well plates to perform the drug treatment. First, drug treatment after homogeneous subculture was performed by seeding 250'000 cells exclusively from the Log phase into six wells of a 6-well plate (Sarstedt GmbH, Nümbrecht, Germany). Cells were counted with a MOXI Z Mini automated cell counter (Orflo Technologies, Ketchum, ID, USA). Additionally, the treatment after heterogeneous subculture was performed by seeding 250'000 cells from the Lag phase, from the Log phase and from the plateau phase each into two wells of a 6-well plate (Figure 1). Each well contained 250'000 cells in 2 mL complete medium.

After seeding, SW480 cancer cells were left to adhere for approximately 21 h. Then, medium was exchanged with solvent control medium or medium containing arsenic trioxide (ATO; Sigma–Aldrich, USA) and incubated for 24 h. ATO stock solutions were prepared according to supplier instructions (pH 7.4). The final ATO concentration (5 µM) was used as previously reported by us.[34] Cell growth and motility was continuously monitored during adhesion and treatments using a PHIO Cellwatcher M and the PHIO Cellwatcher software (Version 2022, PHIO scientific GmbH, Munich, Germany).

Sample work-up. All steps for the sample collection process were performed on ice. The supernatant of each well (2 mL) was transferred into a 15 mL Falcon® tube, centrifuged (1233 g, 5 min, 4 °C) to remove cellular debris and transferred again into a 15 mL Falcon® tube containing ice-cold absolute ethanol (8 mL) and 5 µL of an internal eicosanoid standard mixture (12S-hydroxyeicosatetraenoic acid (HETE)-d8, 15S-HETE-d8, 20-HETE-d6, 5-oxo-eicosatetraenoic acid (ETE)-d7, prostaglandin E2 (PGE2)-d4 and 11,12-dihydroxy-5Z,8Z,14Z-eicosatrienoic acid (DiHETrE)-d11 (Cayman Chemical, Tallinn, Estonia)). The concentrations of the internal standards can be found in Supplementary Information, Table 1. Afterwards, the tube was closed, inverted once and sealed with parafilm. The samples were stored overnight at –20°C and then processed according to the oxylipin and fatty acid analysis protocol.

The adherent SW480 cells were washed twice with cold Tris-buffered saline (TBS; 25 mM Tris·HCl, 150 mM NaCl, pH 7.4) and then, the wash buffer was completely removed. A volume of 80 µL of 4% [wt/vol] sodium deoxycholate lysis buffer (SDC; 0.4 g SDC, 500 µL Tris·HCl (pH 8.8) in 9.5 mL H_2O) was added to the well. The cells were scraped off and the whole cell lysate (WCL) was transferred to an Eppendorf® tube. This step was repeated with 50 µL SDC and the remaining WCL was also added to the corresponding tube, which was subsequently heated to 95 °C for 5 min. These samples were stored at –20 °C until (phospho-)proteomic processing.

Oxylipin and fatty acid analysis

Sample Preparation. The analysis of oxylipins and fatty acids was performed as previously described.[6,43] The eicosanoid samples in Flacon® tubes were centrifuged (30 min, 4536 g, 4 °C) and the clear supernatants were transferred into new 15 mL Falcon® tubes. EtOH was evaporated *via* vacuum centrifugation at 37 °C until the original sample volume (2 mL) was restored. Samples were loaded onto preconditioned StrataX solid-phase extraction (SPE) columns (30 mg mL^{-1}, Phenomenex, Torrance, CA, USA) using Pasteur pipettes. SPE columns were washed with ice-cold H_2O (5 mL, MS grade, VWR International, Vienna, Austria) and elution of analytes was carried out with ice-cold MeOH (500 µL, MS grade, VWR International,

Vienna, Austria) containing 2% formic acid (FA; ≥99%. VWR International, Vienna, Austria). The eluted samples were dried using a gentle nitrogen stream at room temperature. The dried samples were reconstituted in 150 µL reconstitution buffer (H_2O : ACN : MeOH [vol% 65 : 31.5 : 3.5] + 0.2% FA). Then, the samples were directly transferred into an autosampler held at 4 °C and subsequently analyzed *via* LC-MS/MS.

LC–MS/MS Analysis. For the LC-MS analyses, separation of analytes was achieved using a Vanquish™ UHPLC system (Thermo Fisher Scientific™, Vienna, Austria) equipped with a reversed-phase Kinetex® C18 column (2.6 µm XB-C18, 100 Å, LC column 150 × 2.1 mm, Phenomenex, Torrance, CA, USA). Flow rate was set to 200 µL·min^{-1}, the injection volume was 20 µL and all samples were measured in technical duplicates. The LC column oven was set to 40 °C and the autosampler was set to 4 °C. A gradient flow profile was applied (mobile phase A: H_2O + 0.2% FA, mobile phase B: ACN : MeOH [vol% 90 : 10] + 0.2% FA) starting at 35% B and increasing to 90% B (1–10 min). After further increasing to 99% B within 0.5 min and keeping it for 5 min, solvent B was decreased to 35% B within 0.5 min and held for 4 min to equilibrate the column, resulting in a total run time of 20 min. The Vanquish™ UHPLC system was hyphenated to a high-resolution quadrupole orbitrap mass spectrometer (Thermo Fisher Scientific™ QExactive™ HF hybrid quadrupole orbitrap mass spectrometer), which was equipped with a HESI source operating in negative ionization mode. Spray voltage was set to 3.5 kV, capillary temperature was set to 253 °C, sheath gas and auxiliary gas were set to 46 and 10 arbitrary units, respectively. Data were recorded in the scan range of *m/z* 250–700 on the MS1 level with a resolution of 60’000 (*m/z* 200). A Top2 method with a resolution of 15’000 (*m/z* 200) was selected using HCD fragmentation with a normalized collision energy of 24 for data-dependent acquisition. Additionally, an inclusion list was generated with 33 precursor masses, which are specific for oxylipins and their precursor fatty acids (Supplementary Information, Table 2).

LC–MS/MS Data Processing. For the data analysis, raw files generated by the QExactive™ HF hybrid quadrupole orbitrap high-resolution mass spectrometer were checked manually using the Xcalibur™ Qual Browser software (version 4.1.31.9, Thermo Fisher Scientific™, Bremen, Germany) by comparing reference spectra from the LIPIDMAPS depository library from July 2020.[44] In general, identification of analytes was performed using exact mass, retention time and MS/MS fragmentation pattern. For relative quantification, the TraceFinder software (version 4.1, Thermo Fisher Scientific™, Bremen, Germany) was applied, allowing a mass deviation of 5 ppm.

The resulting data containing peak areas of each analyte were loaded into the R software package environment (version 4.2.0)[45] and $\log_2$-transformed. For normalization, the $\log_2$-

transformed mean peak area of the internal standards was subtracted from the log_2-transformed analyte areas to correct for variances arising from sample extraction and LC-MS/MS analysis. Then, each log_2-transformed area was increased by adding (x+20) to obtain a similar value distribution compared to label-free quantification in proteomics.[46] Missing values were imputed using the minProb function of the imputeLCMD package (version 2.1).[47] Volcano plots were produced using the ggplot2 package (version 3.4.0).[48] In an unpaired T-test, p-values <0.05 were considered to indicate statistical significance and the Benjamini-Hochberg procedure was applied as multiple testing correction to all p-values.

Proteomics and Phosphoproteomics

Sample Preparation. Proteomic and phosphoproteomic samples were prepared using a modified version of a previously described protocol[49] and employing an adapted version of the EasyPhos platform.[50] WCLs were thawed and lysed using the S220 Focused-ultrasonicator (Covaris, LLC., Woburn, MA, USA). Protein concentrations were determined *via* bicinchoninic acid assay (BCA)-assay. Between 130–220 µg of protein was reduced and alkylated with tris(2-carboxyethyl)phosphine (TCEP) and 2-chloroacetamide (2-CAM) for 5 min at 45 °C, followed by 18 h digestion with Trypsin/Lys-C (1:100 enzyme-to-substrate ratio) at 37 °C.

An aliquot of 20 µg peptide was taken from each sample for global proteome analysis and dried in a vacuum concentrator. Then, the samples were reconstituted in styrenedivinylbenzene-reverse phase sulfonate (SDB-RPS) loading buffer (99% iPrOH, 1% TFA) and desalted *via* SDB-RPS StageTips. Desalted global proteome samples were reconstituted in 5 µL formic acid (30%) containing synthetic standard peptides at 10 fmol and diluted with 40 µL loading solvent (98% H_2O, 2% ACN, 0.05% TFA).

For phosphopeptide enrichment, the digested samples were mixed with enrichment buffer (52% H_2O, 48% TFA, 8 mM KH_2PO_4) and incubated with TiO_2 Titansphere beads (GL Sciences, Japan), followed by sample clean-up *via* C_8-StageTips. Phosphopeptides were eluted and subsequently dried in a vacuum concentrator. Phosphopeptides were reconstituted in 15 µL MS loading buffer (97.7% H_2O, 2% ACN, 0.3% TFA).

LC-MS/MS analyses. LC-MS/MS analyses were performed employing a timsTOF Pro mass spectrometer (Bruker Daltonics, Bremen, Germany) hyphenated with a Dionex UltiMate™ 3000 RSLCnano system (Thermo Scientific, Bremen, Germany). Samples were analyzed in data-dependent acquisition mode by label free quantification (LFQ) shotgun proteomics similarly to a recently published method.[49] The injection volume was 10 µL and 2 µL for analyzing phosphoproteomes and global proteomes, respectively. Samples were loaded on an Acclaim™PepMap™ C18 HPLC pre-column (2 cm × 100 µm, 100 Å, Thermo

Fisher Scientific™, Vienna, Austria) at a flow rate of 10 µL min^{-1} MS loading buffer. After trapping, peptides were eluted at a flow rate of 300 nL min^{-1} and separated on an Aurora series CSI UHPLC emitter column (25 cm × 75 µm, 1.6 µm C18, Ionopticks, Fitzroy, Australia) applying a gradient of 8–40% mobile phase B (79.9% ACN, 20% H_2O, 0.1% FA) in mobile phase A (99.9% H_2O, 0.1% FA) over 85 min.

Data analysis. Protein identification was performed *via* MaxQuant[51] (version 1.6.17.0) employing the Andromeda search engine against the UniProt Database[52] (version 11/2021, 20'375 entries). Search parameters were set as previously described.[49] A mass tolerance of 20 ppm for MS spectra and 40 ppm for MS/MS spectra, a PSM–, protein– and site-false discovery rate (FDR) of 0.01 and a maximum of two missed cleavages per peptide were allowed. Match-between-runs was enabled with a matching time window of 0.7 min and an alignment time window of 20 min. Oxidation of methionine, N-terminal protein acetylation and phosphorylation of serine, threonine and tyrosine were set as variable modifications. Carbamidomethylation of cysteine was set as fixed modification.

Global proteome data analysis was performed *via* Perseus (version 1.6.14.0). Proteins with at least 60% quantification rate in at least one group were considered for analysis. A two-sided Student's T-test with S0 = 0.1 and a FDR cut-off of 0.05 was applied for identifying multiple testing-corrected significantly regulated proteins.

Phosphoproteomic data processing and analysis was performed according to a modified version of the PhosR protocol[53] employing the R-packages PhosR[54] (version 1.4.0), limma[55] (version 3.50.3) and dplyr[56] (version 1.0.10). Highest intensity values of phosphosites identified in multiple phosphopeptide isoforms were used for analysis. Reverse matches and potential contaminants were filtered. Only class I phosphosites with localization probability ≥0.75 with at least 60% quantification rate in at least one group were considered. Tail-based imputation of missing values was performed and data was centered across their median. Differentially phosphorylated sites between conditions were determined, phosphosites with an adjusted p-value ≤0.05 were considered as significantly regulated. For kinase-substrate mapping, an analysis of variance (ANOVA) test was performed and phosphosites with an adjusted p-value <0.05 and with difference >0 were submitted to the kinaseSubstrateScore function of PhosR with default parameter settings (numMotif = 5, numSub = 1).

Data visualization. If not otherwise specified, data visualization was performed in RStudio[45] (version 2021.09.0) employing the packages ggplot2[48] (version 3.3.6), ggpubr[57] (version 0.4.0), ggrepel (version 0.9.1)[58] and VennDiagram (version 1.7.3).[59]

CausalPath analysis. CausalPath[9] was utilized to analyze causal networks integrating global proteomics and phosphoproteomics using pre-processed LFQ intensity values and standard parameter settings: value transformation = significant-change-of-mean and FDR threshold = 0.1 for protein and phosphoprotein. The resulting networks were visualized in Newt.[60]

Data Availability. All (phospho-)proteomics data was submitted to the ProteomeXchange Consortium (http://proteomecentral.proteomexchange.org) and is available in the PRIDE partner repository[61] with the dataset identifier PXD039768.

Results

Experimental Design to Assess the Memory Effects from Subculture

Cell lines are usually expanded by subdivision of a proliferative cell population and transfer from one culture flask to another, which is known as subculture.[40] The impact of cellular memory effects during subculture was individually assessed by homogeneous and heterogeneous subcultures and subsequent transfer at equal cell numbers to perform the perturbation experiment. The effect of the subculture memory effect was evaluated using multilevel omics and its impact on perturbation networks was determined (Figure 1). First, a homogeneous subculture was generated from SW480 colon carcinoma cells in the Log phase of the growth curve[40] corresponding to 75% growth area occupied by cells. Cells for vehicle controls and treatments were seeded as 250’000 cells into 6-well plates in hexuplicates. Second, a heterogeneous subculture was generated from SW480 cells in the Lag phase, Log phase and plateau phase. Cells in each growth phase were obtained in separate cell culture flasks. Cells from the Lag phase were subcultured at 20% growth area occupied, while cells from the plateau phase were subcultured at >95% growth area occupied, the latter reflecting density limitation of cell proliferation.[40] Again, an equal number of 250’000 cells from the three growth phases were seeded into individual 6-well plates in duplicates (Figure 1). The drug treatment was carried out identically after both homogeneous and heterogeneous subcultures. The cells were left to adhere for 21 h. Then, the medium was exchanged and cells were either treated with vehicle control or drug (5 µM) for 24 h. The perturbation was induced with arsenic trioxide (ATO), a clinically approved anticancer agent for the treatment of acute promyelocytic leukemia,[38,39] which shows a multimodal MoA in cancer cells.[34,35,62,63]

After the incubation period, the samples from homogeneous and heterogeneous subcultures were processed to enable a multilevel omics analysis.[6,43] Oxylipins and fatty acids were isolated from supernatants by first precipitating cell debris and proteins and subsequently perform a solid-phase extraction. The protein fraction was obtained from whole cell lysates (WCLs) and used for global proteomics and phosphoproteomics. WCLs were homogenized for down-stream protein quantification. They were proteolytically digested and subsequently underwent phosphopeptide enrichment using TiO_2 beads.[49] Thereafter, oxylipins and fatty acids, as well as global proteomes and phosphoproteomes were analyzed by dedicated liquid-chromatography tandem mass spectrometry (LC-MS/MS) methods on different platforms in a data-dependent analysis mode. All reported p-values were multiple testing corrected using FDR calculations and the significantly regulated molecular events are listed in the Supplementary Tables 1 and 2. Additionally, the cell growth and motility was continuously assessed throughout the adhesion and incubation period in each well by means of a Cellwatcher M, which combines six microscope units in one device and is compatible with 6-well plates. Bilevel perturbation networks of the ATO-treated homogeneous and heterogeneous subcultures were constructed from the proteomic and phosphoproteomic data.[9]

Impact of Subculture Memory Effect on Cell Growth and Motility

Cell growth and motility was continuously monitored using the Cellwatcher over the entire adhesion and treatment incubation periods. The memory effects from subculture can be clearly illustrated by the growth area occupied by cells. After both the homogeneous and heterogeneous subcultures, the cells were seeded at around 10% growth area occupied. The cells were monitored directly after seeding. The increase in growth area occupied over the first 20 h relates to cell spreading and proliferation. Crucially, despite being seeded at equal cell numbers, cell growth after homogeneous subculture is much more uniform among the individual replicates (Figure 2A) compared to cell growth after heterogenous subculture (Figure 2B), while the effect of the ATO-treatment showed an immediate growth inhibition after both subculture conditions. At the last analysis time point before work-up, the control cells showed 89±5% (CV = 5%) and 84±11% (CV = 13%) growth area occupied after homogeneous and heterogeneous subculture, respectively. The treatment clearly reduced cell growth to 57±4% (CV = 7%) after homogeneous subculture, while this effect was less pronounced after heterogeneous subculture showing 77±18% (CV = 23%) growth area occupied.

Transformed cells typically display random migration, which can be determined by means of time-lapse microscopy. Cell motility depends on the cell density in the plate, but also on drug treatments. At the last analysis time point before work-up, the control cells displayed a mean cell motility 5.6±0.2 $\mu m \cdot h^{-1}$ and 5.5±0.7 $\mu m \cdot h^{-1}$ after homogenous and heterogenous

subculture, respectively. ATO-treated cells showed a reduced motility of 4.0±0.2 $\mu m \cdot h^{-1}$ and 1.9±0.2 $\mu m \cdot h^{-1}$ after homogenous and heterogenous subcultures, respectively (Figure 2C and 2D; Supplementary Information, Figure 2). The drug treatment led to a substantial decrease in cell motility irrespective of the subculture condition. However, the mode of subculture manifested in the variation of cell motility among replicates. The homogeneous subculture delivered a reduced variation of the biological replicates compared to the heterogeneous subculture. The controls from homogeneous subculture displayed a coefficient of variation (CV) of 4% of cell motility at the last time point before work-up, while the controls from heterogeneous subculture showed an enhanced CV of 12%. The impact of subculture was similar for the treated cells, where the homogeneous and heterogeneous subcultures yielded CVs of 5% and 10%, respectively.

Impact of Subculture Memory Effect on Oxylipins and Fatty Acids

Oxylipins and fatty acids were isolated from the supernatants of control and ATO-treated SW480 cancer cells. Any down- or upregulation thereby indicates their consumption or release, respectively.[43] A total of 87 oxylipins and fatty acids were identified in the entire data set of both homogeneous and heterogeneous subculture conditions, together with 27 eicosanoid features. Of the 87 identified oxylipins and fatty acids, 31 were significantly upregulated upon treatment with ATO after homogeneous subculture, while only 10 lipid species were upregulated after heterogeneous subculture. Of the significantly upregulated lipid species, 10 were found after both homogeneous and heterogeneous subculture. (Figure 3A).

Principal component analysis (PCA) showed a reduced variation of biological replicates of eicosadomic profiles after homogeneous subculture compared to heterogeneous subculture (Figure 3B). Accordingly, control and ATO-treated samples were better separated after the homogeneous subculture, while samples corresponding to the respective conditions were found more dispersed after the heterogeneous subculture and overlapped considerably.

The median coefficient of variation (CV) of normalized intensity values between biological replicates of the control group was 1% after homogeneous subculture and 3% after heterogeneous subculture (Figure 3C). Regarding regulations of eicosanoids and their precursors upon ATO treatment, median $\log_2$ fold-changes after the homogeneous and heterogeneous subcultures were 0.43 and 0.27, respectively. Median $-\log_{10}$-adjusted (adj.) p-values accounted for 2.3 and 0.8 after the homogeneous and heterogeneous subcultures, respectively.

Upon ATO treatment, 31 lipid species were significantly upregulated (adj. p-value ≤0.05, FC ≥2), while none were significantly down-regulated after homogeneous subculture. After the heterogeneous subculture, 10 lipid species were significantly upregulated upon ATO treatment, and none were down-regulated (Figure 3D).

Arachidonic acid (AA) was among the shared upregulated lipid species in both subcultures upon ATO treatment. AA is the precursor of most eicosanoids[64] and it was found significantly upregulated 18– (CV = 3%, $-\log_{10}$-adj. p-value = 9.5) and 4-fold (CV = 8%, $-\log_{10}$-adj. p-value = 2.6) in the homogeneous and heterogeneous subcultures, respectively. The non-enzymatically formed 9-hydroxyeicosatetraenoic acid (9-HETE) is an oxidative stress marker.[65] It was significantly upregulated only in the homogeneous subculture (FC = 3.9, CV = 2%, $-\log_{10}$-adj. p-value = 14.5), but not in the heterogeneous subculture (FC = 1.2, CV = 4%, $-\log_{10}$-adj. p-value = 0.8). In addition, the epoxyeicosatrienoic acids (EETs) are cytochrome P450 oxidation products of AA with anti-apoptotic and anti-oxidative effects.[66] The identified 5(6)-EET and 14(15)-EET were significantly upregulated 10.8– ($-\log_{10}$-adj. p-value = 7.4) and 4.5-fold ($-\log_{10}$-adj. p-value = 8.7) in the homogeneous subculture upon ATO treatment, respectively. The CV of the control samples was 1% for both EETs. In contrast, those EETs were not significantly regulated in the heterogeneous subculture upon ATO treatment. Under these conditions, 5(6)-EET showed a fold-change of 2.1 (CV = 11%, $-\log_{10}$-adj. p-value = 1) and 14(15)-EET a fold-change of 1.1 (CV = 9, $-\log_{10}$-adj. p-value = 0.1).

Impact of Subculture Memory Effect on Proteomics

The proteomic analysis of whole cell lysates resulted in the identification of a total of 4554 and 4445 proteins after the homogeneous and the heterogeneous subculture, respectively. A total of 4291 proteins were identified after both the homogeneous and heterogeneous subcultures, while 263 and 154 proteins were exclusively identified after the respective subcultures (Figure 4A). Consequently, 94% of proteins identified after the homogeneous and 97% of proteins identified after the heterogeneous subculture were also identified in the respective other group.

Of the 343 distinctly upregulated proteins upon treatment with ATO, 106 (31%) were upregulated after both subculture conditions, while approximately the same numbers were upregulated in one specific subculture condition. A more pronounced contrast was evidenced for the down-regulated proteins, where 83 (12%) proteins of a total of 681 down-regulated proteins were shared between the two subculture conditions. Moreover, the homogeneous subculture displayed 458 uniquely down-regulated proteins compared to 140 in the heterogeneous subculture.

The PCA showed an reduced variation of biological replicates of proteomic profiles after the homogeneous compared to the heterogeneous subculture (Figure 4B). Accordingly, control and ATO-treated samples were clearly separated after the homogeneous subculture,

while samples corresponding to the respective conditions were found more dispersed after the heterogeneous subculture with a partial overlap.

The median CV of protein LFQ intensity values among biological replicates of the control group was 11% after the homogeneous subculture and 23% after the heterogeneous subculture (Figure 4C). Regarding protein regulations upon ATO treatment, the median log_2 fold-change after homogeneous and heterogeneous subculture was –0.13 and 0.01, respectively. The median $–log_{10}$-adj. p-value accounted for 1.3 and 0.7 after the homogeneous and heterogeneous subcultures, respectively.

Upon ATO treatment, 243 proteins were significantly upregulated (adj. p-value ≤0.05, fold-change (FC) ≥1) and 541 proteins significantly down-regulated (adj. p-value ≤0.05, FC ≤1) after the homogeneous subculture. After the heterogeneous subculture, 206 and 223 proteins were significantly up- and down-regulated upon ATO treatment, respectively. The protein Heme oxygenase 1 (HMOX1), which is involved in protection of cells against oxidative stress and apoptosis,[67-69] was significantly upregulated after both the homogeneous and the heterogeneous subcultures, exhibiting $–log_{10}$-adj. p-values of 11.2 and 3.9 and log_2 fold-changes of 9.9 and 6.33, respectively (Figure 4D).

Impact of Subculture Memory Effect on Phosphoproteomics

The phosphoproteomic analysis resulted in the identification of 2278 and 2082 class I phosphosites with localization probability ≥75% after the homogeneous and the heterogeneous subculture, respectively.

The number of phosphosites identified after both subcultures was 1812, corresponding to 71% of the total phosphosites (Figure 5A). A total of 466 and 270 phosphosites were uniquely identified after the homogeneous and heterogeneous subcultures, respectively. Of the 618 significantly upregulated phosphosites only 32 (5%) were shared between the two subculture conditions, while 538 phosphosites were uniquely upregulated after the homogeneous subculture and 48 were uniquely upregulated after the heterogeneous subculture. A similar amount corresponding to 29 (9%) of a total of 312 phosphosites were significantly down-regulated after both subculture conditions, while 134 phosphosites were uniquely down-regulated after the homogeneous subculture and 149 were uniquely down-regulated after the heterogeneous subculture.

The PCA of the phosphoproteomics showed that biological replicates from the heterogeneous subculture were more dispersed compared to the biological replicates of the homogeneous subculture (Figure 5B). Similarly, ATO-treated samples were clearly separated

from the control samples after homogeneous subculture, whereas samples from the respective conditions overlapped considerably after heterogeneous subculture.

The median CV of phosphosite LFQ intensity values among the biological replicates of the control group was 24% after homogeneous subculture and 53% after heterogeneous subculture (Figure 5C). The median $\log_2$ fold-change of phosphosites upon ATO treatment was 0.42 and –0.24 within the homogeneous and heterogeneous subculture, respectively. The median $-\log_{10}$-adj. p-value accounted for 0.7 and 0.5 after the homogeneous and heterogeneous subculture, respectively.

In the samples after the homogeneous subculture, 570 phosphosites were found significantly upregulated upon ATO treatment (adj. p-value ≤0.05), whereas 163 phosphosites were significantly down-regulated (adj. p-value ≤0.05, Figure 5D). In contrast, after heterogeneous subculture, only 80 phosphosites were found to be significantly upregulated upon ATO treatment, whereas 178 phosphosites were significantly downregulated.

The significantly upregulated phosphosites were mapped to potential kinases *via* the kinase substrate scoring function of PhosR[54] based on their dynamic phosphorylation profiles and kinase recognition motifs. This combined score includes a minimum of 5 sequences used for compiling the motif for each kinase and minimum of one phosphosites for compiling phosphorylation profiles for each kinase. A heatmap of the combined scores retrieved for the top three phosphosites with the highest combined scores of all evaluated kinases is shown in Supplementary Information, Figure 3. The mapping of significantly upregulated phosphosites after the homogeneous subculture resulted in the annotation of 40 kinases to their corresponding top 3 scoring phosphosites (Supplementary Information, Figure 3A), whereas 19 kinase-top three substrate pairs were mapped after the heterogeneous subculture (Supplementary Information, Figure 3B).

Impact of Subculture Memory Effect on the Perturbation Network

CausalPath analysis[9] integrated proteomic and phosphoproteomic analyses into a bilevel causal perturbation network. After homogeneous subculture a total of 321 causal conjectures were identified (Figure 6A), while 58 causal conjectures were observed after heterogeneous subculture in their respective perturbation networks (Figure 6B). The majority of the causal conjectures found in the perturbation network after heterogeneous subculture were also found in the one after homogeneous subculture. Of these shared conjectures, the directions of individual protein regulation and (de-)phosphorylation events were also similar.

ATO is known to exert pleiotropic effects by inducing multiple signalling cascades and affecting numerous cellular functions.[35,63] Notable contributors to the MoA beyond PML-RARα degradation include the induction of reactive oxygen species (ROS), protein kinase signalling, heat shock proteins, apoptosis, as well as the disruption of the cell cycle.[35,63] Both perturbation

networks featured robust ATO-induced expression changes and phosphorylation events that are coordinated by the transcription factor MYC (Figure 6).[63] ATO treatment activated MAPK1, which directly phosphorylated MYC[70] and this is paralleled by EGFR activation.[71] Arsenic is known to decrease transcription by direct effects on the transcription factors SP1 and MYC,[72,73] and this seems to be further supported by the upregulation of ZFP36L1,[74] which mediates RNA decay. Moreover, a reduced transcriptional activity of MYC led to the upregulation of the transcriptional repressor HBP1, which plays a role in cell cycle regulation by down-regulating the S-phase associated DNA methyltransferase DNMT1.[75] Similarly, ATO induced the expression of GADD45A[76] and cyclin D1 (CCND1),[72] which are regulators of the G2/M and G1/S transitions, respectively. DNA damage repair signatures were characterized by the down-regulation of MSH2[77] and FANCD2. Next to initiating MAP signal transduction pathways, ATO induced several heat shock proteins, including HSP90AA1, HSPD1 and HSPA4. HSP90AA1 (HSP90) is the most abundant chaperone and seems to be inhibited by arsenite[78] and HSPD1 (HSP60) was shown to be a direct target of ATO.[79] Additionally, as part of the stress response, HMOX1[35] and NDRG1 were also found upregulated upon ATO treatment in both perturbation networks, the latter being necessary for p53-dependent apoptosis.[80] ATO also induced the death receptors TNFRSF10B and TNFRSF10D.[81] The upregulation of the casein kinase II subunit alpha (CSNK2A1)[82] was observed and led to the phosphorylation of a number of substrates in both perturbation networks, *e.g.* a deactivating phosphorylation on catenin alpha-1 (CTNNA1), which affects the actin network and cadherin-cell adhesion properties. Accordingly, the cytoskeleton was suggested as a mediator of the MoA of ATO.[63] Both perturbation networks displayed an increased CDK6 expression in response to decreased MYC activity, which in turn led to phosphorylation events on zyxin (ZYX), an adhesion plaque protein that mediates adhesion-stimulated changes in gene expression. All these changes can be directly related to the known intracellular effects of ATO.[35,63]

In contrast to these similarities, the perturbation networks also showed specific responses to the ATO treatment depending on the subculture conditions. The perturbation network after homogeneous subculture yielded numerous additional causal conjectures compared to the one after heterogeneous subculture. This enhanced the information density in the network and highlighted additional transcription factor hubs and signalling events (Figure 6A). In addition to MYC, the transcription factor SP1[73] was down-regulated. SP1 coordinated the down-regulation of 17 gene-expression products, including DNMT1, and the up-regulation of SOD1, SOD2,[83] and EGFR. This perturbation network also displayed activating phosphorylations on EGFR next to its upregulation.[71] Additional down-regulated transcription factors not yet implicated in ATOs MoA included MAX, TFDP1 and RB1, the latter featured decreased phosphosite occupancy.[84] RB1 is a tumour suppressor protein that is tightly linked to cell cycle regulation[85] and connected to CDK1 and CDK5 via phosphorylation events. Arsenite is known to activate

the transcription factor AP-1 by increasing the expression of the mitogenic components JUN and FOS.[86] Those were exclusively observed in the perturbation network after homogeneous subculture and were upregulated in contrast to the other transcription factors. Phosphorylation of JUN was mediated by MAPK1 and MAPK3, which themselves were detected containing activating phosphorylations. The phosphorylation of MAPK1 seemed to be caused by the stress-activated MAP2K3, NRAS, the RAS-related protein RAP1A and LYN, which itself features a phosphorylation event. Activated MAPK1 also led to the hyperphosphorylation of the microtubulin-binding protein MAP1B that may reflect cytoskeletal adaptions.[63] Upregulated AP-1 also induced RHOA signalling,[35] which is exclusively observed in this perturbation network. The upregulation of CSNK2A1 was paralleled by upregulated CSNK2A2 and down-stream phosphorylation of 15 substrates compared to 2 substrates in the perturbation network after heterogeneous subculture.

The perturbation network after heterogeneous subculture featured only limited specific effects featuring STAT3 as a second hub of controlling gene expression. However, this transcription factor was not detected in the data set and was annotated by the CausalPath algorithm based on the upregulation of a number of down-stream gene expression products (Figure 6B). The effect of arsenic on STAT3 seems to be highly context-dependent.[87,88] A further down-regulated DNA damage signature including PRKDC and the concomitant dephosphorylation of XRCC4 was observed, which are involved in non-homologous end joining.

Discussion

MS-based omics techniques are valuable tools for drug discovery.[1,5] They allow to construct perturbation networks that aid in MoA deconvolution, which is additionally facilitated by multilevel omics combinations,[8,89] increasing the number of perturbations[4] or by attempts of causal reasoning.[9] Importantly, the quality of the perturbation network is strongly determined by experimental and sample processing workflows that give rise to an overall variation, expressed as CV, which defines the experimental reproducibility. The impact of cell culture conditions on cellular functions and the reproducibility of omics readouts is a current topic of investigation.[17,30,31] Approaches to account for the genetic evolution of cells in culture *via* cellular force tracking exist and provide quantitative data.[90] Here, we demonstrate that memory effects of cancer cells from subculture directly impact on the variation of multilevel omics readouts and on cell growth and motility as a phenotypic parameter, but not necessarily on the effect size. The same effects were evidenced for statistical evaluations based on linear modelling (Limma)[55] and permutation-based FDR (Perseus)[91] calculations.

Two different subculture conditions were established to assess the memory effect of SW480 colon cancer cells on drug-induced perturbation networks (Figure 1). First, a homogeneous subculture consisting of cells in the Log phase of cell growth was generated. Second, a heterogeneous subculture condition was generated using cells of different phases of cell growth, including Lag phase, Log phase and plateau phase, each in duplicates. Equal number of cells of the three growth phases were seeded in individual 6-well plates. Control and drug-treatments were performed in hexuplicates after both subculture conditions. The cells were drug-treated for 24 h and cell growth and motility were continuously monitored. Thereafter, each sample was processed to allow for multilevel omics analysis. Oxylipins and fatty acids were obtained from supernatants. Global proteomics and phosphoproteomics were assessed from WCLs. The impact of these subculture conditions on each omics level and on cell motility was monitored with respect to number of identified molecules, number of significantly regulated molecules, homogeneity of the omics profile *via* principal component analysis (PCA), as well as overall CV, effect size (fold-change, FC) and significance (FDR-adjusted p-values). Finally, the impact of the two subculture conditions on the perturbation network was evaluated. Perturbations were induced by arsenic trioxide (ATO). ATO is an intriguing anticancer metalloid that cures patients suffering from acute promyelocytic leukaemia in combination with all-*trans* retinoic acid.[39,92] Its clinically relevant MoA includes the degradation of the oncogenic PML-RARα fusion protein that relieves the differentiation blockade of the premature cancerous blasts.[38] In solid tumors, ATO was shown to exert pleiotropic effects based on the induction of ROS, heat shock proteins, kinase signaling and apoptosis and therefore, represents a good model drug for this multilevel omics study.[63]

Strikingly, the homogeneous subculture yielded a reduced variation across all phenotypic and molecular readouts compared to the heterogeneous subculture. For example, cell growth and motility were reduced upon ATO treatment under both conditions, but the variation of controls and treatments were considerably larger after the heterogeneous subculture (Figure 2). Cell growth also illustrates the memory effect of the subculture conditions since the initial growth area occupied was around 10% in all cases by seeding always the same number of cells (Figure 2A and 2B). Importantly, cell growth and motility were much more uniform after homogeneous compared to heterogeneous subculture.

While the subculture conditions affected the number of identified molecules in the eicosadomics, proteomic and phosphoproteomic analyses only to a minor degree (Figures 3A–5A), they considerably affected the number of significantly regulated molecules in favor of the treatment after homogeneous subculture on all levels up to 7-fold, as exemplified by the upregulated phosphosites (Figure 5A). The profiles of the samples after homogeneous subculture were also more uniform on all omics levels and irrespective of control or treatment conditions compared to samples after heterogeneous subculture as evidenced in the PCA

plots (Figures 3B–5B). This resulted in an improved group separation. Consequently, on all omics levels, the homogeneous subculture yielded higher significance values compared to the heterogeneous subculture in the drug treatment (Figures 3C–5C). Since the overall fold-changes after the subculture conditions were only affected to a minor degree, this effect can be mainly attributed to a decreased CV after homogeneous subculture. The CVs decreased from 3% to 1% in the eicosadomic, from 23% to 11% in the proteomic and from 53% to 24% in the phosphoproteomic analysis when comparing controls obtained from the heterogeneous to the homogeneous subculture, respectively. This effect manifested also in the volcano plots on all molecular levels (Figures 3D–5D).

Consequently, a larger number of significantly regulated eicosanoids and their precursors were observed under homogeneous compared to heterogeneous conditions. Only the former revealed lipid species related to the ATO treatment. For example, 9-HETE was upregulated and represents a marker for oxidative stress.[65] This eicosanoid is formed non-enzymatically from AA. Furthermore, the P450-products 5(6)-EET and 14(15)-EET were found upregulated and those were shown to exhibit anti-apoptotic and anti-oxidative effects.[66]

As evidenced by the eicosadomics data, the increase of the number of significant molecular events may precipitate in a higher information density to delineate MoA of drugs and investigative drug candidates. Bilevel perturbation networks were generated for the treatments after the two subculture conditions from the proteomics and phosphoproteomics experiments using CausalPath.[9] Indeed, ATO-treatment after homogeneous subculture generated 321 causal conjectures, while the treatment after heterogeneous subculture yielded 58 causal conjectures. Both perturbation networks confirmed essentially the multi-modal MoA of ATO (Figure 6).[63] We observed an induction of HMOX1,[35] as well as the heat shock proteins HSP90AA1,[78] HSPD1[79] and HSPA4, which indicate the generation of ROS by ATO. ATO treatment was found to activate MAPK1.[63] This in turn led to phosphorylations on the transcription factor MYC,[70] which is an important regulator of cell fate and directly controls heat shock protein expression. Phosphorylation of MYC at serine-62[93] was identified as an important initial effect of ATO after both subculture conditions (Figure 6; Supplementary Information, Figure 3). The impact of ATO on the cell cycle was evidenced by the induced expression of GADD45A[76] and CCND1,[72] which are regulators of cell cycle transitions. Apoptotic signals were not observed on the protein levels because we used sub-cytotoxic concentrations of ATO.[35]

Despite the still successful MoA deconvolution of ATO after the heterogeneous subculture, the homogeneous subculture provided an enhanced information density in the perturbation network on the levels of expression changes and phosphorylation events. This can be exemplified by the additional observation of the transcription factors SP1[73] and AP-1[63,86] as hubs for mediating ATO-induced gene expression changes, and by numerous cell cycle

regulators (Figure 6A). Despite an upregulation of MAPK1 as detected after the heterogeneous subculture, the homogeneous subculture was characterized by activating phosphorylations on MAPK1 by LYN, which was itself phosphorylated. The causal network also revealed so far unprecedented effects of ATO, including the down-regulation of the transcription factors Max, TFDP1 and RB1. Interestingly, RB1 is directly involved in the regulation of the cell cycle[85] and shows four dephosphorylation events.[84] Phosphorylation of RB1 is known to inhibit its function.[94]

Finally, a number of cellular pathways affected by the ATO-treatment were not identifiable directly in the perturbation network, but only *via* manual data interpretation. Among these was the induction of the cytoprotective Nrf2-mediated oxidative stress response, which was previously shown as a relevant resistance pathway against ATO.[95] First, we found Cullin-3 (CUL3) to be induced upon ATO-treatment, which contributes towards the degradation of Nrf2 at resting state, but only after homogeneous subculture.[95] Moreover, several canonical Nrf2-target genes were induced upon drug treatment after both subculture conditions, including HMOX1, SQSTM1, SRXN1, GCLM, as well as the ferritin components FTL and FTH1, among others (Supplementary Information, Figure 4A). Again, additional Nrf2-target genes were observed after homogeneous subculture in the same setup, including TXNRD1, GSTM4 and the oxidative stress-induced growth inhibitor 1 (OSGIN1), which may be an indicator for the apparent stress-induced cell cycle arrest. Oxidative stress may eventually lead to DNA damage. However, an ATO-induced DNA damage response was not observed. Oxidative stress on DNA may have been limited by the action of abasic site processing protein HMCES, an ancient DNA lesion recognition protein preserving genome integrity.[96] This suicide enzyme was found stably expressed in most control cells independently of subculture, but vanished in virtually all ATO-treated cells (Supplementary Information, Figure 4B). The DNA excision repair enzymes GADD45A, GADD45B, both significantly upregulated by ATO (Figure 6), may have additionally supported the preservation of genome integrity. These findings highlight the value of manual data interpretation to complement computational data-mining and at the same time, the need for improvements in databases with respect to stress response pathways.

Conclusions

While confluence dependencies and phenotypic switches in cell culture are known to impact on the quality of omics experiments, this study quantifies the influence of memory effects of subculture conditions on multilevel omics readouts for drug discovery. A clear decrease in experimental variation on eicosadomics, proteomics and phosphoproteomics levels was observed for the drug-treatment after homogeneous subculture, which consisted of cells

exclusively from the Log phase compared to heterogeneous subculture, which consisted of cells from Lag, Log and plateau phases of growth. Yet, the subculture conditions did not considerably affect the number of identified molecules, nor the fold-change distributions of the perturbations. Therefore, the reduced number of significantly regulated molecules after heterogeneous subculture was primarily attributed to the enhanced experimental variation. Importantly, the treatment after heterogenous subculture still enabled deconvoluting the established MoA of arsenic trioxide, but an enhanced information density was observed after homogeneous subculture that enabled a more detailed MoA confirmation and the discovery of unprecedented drug effects. Consequently, this study sheds light onto how to control subculture conditions to maximize MoA deconvolution and is of broad relevance to omics-based drug discovery because these effects were observed not only on the molecular level in supernatants and WCLs, but also on the phenotypic levels of cell growth and motility. Finally, the information density of perturbation networks may not only inform drug MoAs, but may also be used for plausibility assessment and quality control of the perturbation study.

Acknowledgements

The authors are grateful to the Core Facility of Mass Spectrometry at the Faculty of Chemistry and the Joint Metabolome Facility, members of the Vienna Life-Science Instruments (VLSI). The authors are grateful to Lion Gleiter for assistance with the data evaluation of the Cellwatcher. Figures were created and assembled using BioRender.com.

Conflict of interest

The authors declare that the research was conducted in the absence of any commercial or financial relationships that could be construed as a potential conflict of interest.

Author contributions

LS performed cell culture, sample workup and Cellwatcher acquisition. PB performed proteomics and phosphoproteomics. GH performed oxylipin and fatty acid analysis. AB and PB acquired and processed data. VP, LG and TM processed data. PB assembled figures. CG, SMM and PP planned and supervised the study. PB, GH, LS, VP, CG and SMM wrote the initial draft of the manuscript, which was edited and approved by all authors.

References

1. Meissner, F.; Geddes-McAlister, J.; Mann, M.; Bantscheff, M., The emerging role of mass spectrometry-based proteomics in drug discovery. *Nat. Rev. Drug Discov.* **2022,** *21* (9), 637-654.
2. Paananen, J.; Fortino, V., An omics perspective on drug target discovery platforms. *Brief. Bioinform.* **2020,** *21* (6), 1937-1953.
3. Matthews, H.; Hanison, J.; Nirmalan, N., “Omics”-informed drug and biomarker discovery: Opportunities, challenges and future perspectives. *Proteomes* **2016,** *4* (3), 28.

4. Ruprecht, B.; Di Bernardo, J.; Wang, Z.; Mo, X.; Ursu, O.; Christopher, M.; Fernandez, R. B.; Zheng, L.; Dill, B. D.; Wang, H., et al., A mass spectrometry-based proteome map of drug action in lung cancer cell lines. *Nat. Chem. Biol.* **2020,** *16* (10), 1111-1119.
5. Skos, L.; Borutzki, Y.; Gerner, C.; Meier-Menches, S. M., Methods to identify protein targets of metal-based drugs. *Curr. Opin. Chem. Biol.* **2023,** *73*, 102257.
6. Kovarik, J. J.; Bileck, A.; Hagn, G.; Meier-Menches, S. M.; Frey, T.; Kaempf, A.; Hollenstein, M.; Shoumariyeh, T.; Skos, L.; Reiter, B., et al., A multi-omics based anti-inflammatory immune signature characterizes long COVID-19 syndrome. *iScience* **2023,** *26* (1), 105717.
7. Montaner, J.; Ramiro, L.; Simats, A.; Tiedt, S.; Makris, K.; Jickling, G. C.; Debette, S.; Sanchez, J.-C.; Bustamante, A., Multilevel omics for the discovery of biomarkers and therapeutic targets for stroke. *Nat. Rev. Neurol.* **2020,** *16* (5), 247-264.
8. Wang, H.; Zhou, Y.; Xu, X.; Li, H.; Sun, H., Metalloproteomics in conjunction with other omics for uncovering the mechanism of action of metallodrugs: Mechanism-driven new therapy development. *Curr. Opin. Chem. Biol.* **2020,** *55*, 171-179.
9. Babur, Ö.; Luna, A.; Korkut, A.; Durupinar, F.; Siper, M. C.; Dogrusoz, U.; Vaca Jacome, A. S.; Peckner, R.; Christianson, K. E.; Jaffe, J. D., et al., Causal interactions from proteomic profiles: Molecular data meet pathway knowledge. *Patterns* **2021,** *2* (6), 100257.
10. Dugourd, A.; Kuppe, C.; Sciacovelli, M.; Gjerga, E.; Gabor, A.; Emdal, K. B.; Vieira, V.; Bekker-Jensen, D. B.; Kranz, J.; Bindels, E. M. J., et al., Causal integration of multi-omics data with prior knowledge to generate mechanistic hypotheses. *Mol. Sys. Biol.* **2021,** *17* (1), e9730.
11. Noble, W. S., How does multiple testing correction work? *Nat. Biotechnol.* **2009,** *27* (12), 1135-1137.
12. Benjamini, Y.; Hochberg, Y., Controlling the false discovery rate: A Practical and powerful approach to multiple testing. *J. R. Stat. Soc. Series B Stat. Methodol.* **1995,** *57* (1), 289-300.
13. Ho, J.; Tumkaya, T.; Aryal, S.; Choi, H.; Claridge-Chang, A., Moving beyond P values: data analysis with estimation graphics. *Nat. Methods.* **2019,** *16* (7), 565-566.
14. Petyuk, V. A.; Gatto, L.; Payne, S. H., Reproducibility and transparency by design. *Mol. Cell Proteomics* **2019,** *18* (8), S202-S204.
15. EURACHEM, Ellison, S. L. R.; WIlliams, A., Eds. *Quantifying uncertainty in analytical measurement*. Third Edition; 2012.
16. Poulos, R. C.; Hains, P. G.; Shah, R.; Lucas, N.; Xavier, D.; Manda, S. S.; Anees, A.; Koh, J. M. S.; Mahboob, S.; Wittman, M., et al., Strategies to enable large-scale proteomics for reproducible research. *Nat. Commun.* **2020,** *11*, 3793.
17. Tabb, D. L.; Vega-Montoto, L.; Rudnick, P. A.; Variyath, A. M.; Ham, A.-J. L.; Bunk, D. M.; Kilpatrick, L. E.; Billheimer, D. D.; Blackman, R. K.; Cardasis, H. L., et al., Repeatability and reproducibility in proteomic identifications by liquid chromatography−tandem mass spectrometry. *J. Proteome Res.* **2009,** *9* (2), 761-776.
18. Sobus, J. R.; Grossman, J. N.; Chao, A.; Singh, R.; Williams, A. J.; Grulke, C. M.; Richard, A. M.; Newton, S. R.; McEachran, A. D.; Ulrich, E. M., Using prepared mixtures of ToxCast chemicals to evaluate non-targeted analysis (NTA) method performance. *Anal. Bioanal. Chem.* **2019,** *411* (4), 835-851.
19. Amaral, O. B.; Neves, K., Reproducibility: Expect less of the scientific paper. *Nature* **2021,** *597* (7876), 329-331.
20. Errington, T. M.; Denis, A.; Perfito, N.; Iorns, E.; Nosek, B. A., Challenges for assessing replicability in preclinical cancer biology. *eLife* **2021,** *10*, 67995.
21. Errington, T. M.; Mathur, M.; Soderberg, C. K.; Denis, A.; Perfito, N.; Iorns, E.; Nosek, B. A., Investigating the replicability of preclinical cancer biology. *eLife* **2021,** *10*, 71601.
22. Rodgers, P.; Collings, A., What have we learned? *eLife* **2021,** *10*, 75830.
23. Baker, M., 1,500 scientists lift the lid on reproducibility. *Nature* **2016,** *533* (7604), 452-454.
24. Meier-Menches, S. M.; Neuditschko, B.; Zappe, K.; Schaier, M.; Gerner, M. C.; Schmetterer, K. G.; Del Favero, G.; Bonsignore, R.; Cichna-Markl, M.; Koellensperger, G., et al., An organometallic gold(I) bis-N-heterocyclic carbene complex with multimodal activity in ovarian cancer cells. *Chem. Eur. J.* **2020,** *26* (67), 15528-15537.
25. Tahir, A.; Bileck, A.; Muqaku, B.; Niederstaetter, L.; Kreutz, D.; Mayer, R. L.; Wolrab, D.; Meier, S. M.; Slany, A.; Gerner, C., Combined proteome and eicosanoid profiling approach for revealing implications of human fibroblasts in chronic inflammation. *Anal. Chem.* **2017,** *89* (3), 1945-1954.
26. Franzke, B.; Bileck, A.; Unterberger, S.; Aschauer, R.; Zöhrer, P. A.; Draxler, A.; Strasser, E.-M.; Wessner, B.; Gerner, C.; Wagner, K.-H., The plasma proteome is favorably modified by a high protein diet but not by additional resistance training in older adults: A 17-week randomized controlled trial. *Front. Nutr.* **2022,** *9*, 925450.
27. Klont, F.; Bras, L.; Wolters, J. C.; Ongay, S.; Bischoff, R.; Halmos, G. B.; Horvatovich, P., Assessment of sample preparation bias in mass spectrometry-based proteomics. *Anal. Chem.* **2018,** *90* (8), 5405-5413.
28. Sitnikov, D. G.; Monnin, C. S.; Vuckovic, D., Systematic assessment of seven solvent and solid-phase extraction methods for metabolomics analysis of human plasma by LC-MS. *Sci. Rep.* **2016,** *6* (1), 38885.
29. Paulitschke, V.; Eichhoff, O.; Gerner, C.; Paulitschke, P.; Bileck, A.; Mohr, T.; Cheng, P. F.; Leitner, A.; Guenova, E.; Saulite, I., et al., Proteomic identification of a marker signature for MAPKi resistance in melanoma. *EMBO J.* **2019,** *38* (15).
30. Liu, Y.; Mi, Y.; Mueller, T.; Kreibich, S.; Williams, E. G.; Van Drogen, A.; Borel, C.; Frank, M.; Germain, P.-L.; Bludau, I., et al., Multi-omic measurements of heterogeneity in HeLa cells across laboratories. *Nat. Biotechnol.* **2019,** *37* (3), 314-322.
31. Niederstaetter, L.; Neuditschko, B.; Brunmair, J.; Janker, L.; Bileck, A.; Del Favero, G.; Gerner, C., Eicosanoid content in fetal calf serum accounts for reproducibility challenges in cell culture. *Biomolecules* **2021,** *11* (1), 113.

32. Lee, A. P.; Kok, Y. J.; Lakshmanan, M.; Leong, D.; Zheng, L.; Lim, H. L.; Chen, S.; Mak, S. Y.; Ang, K. S.; Templeton, N., et al., Multi-omics profiling of a CHO cell culture system unravels the effect of culture pH on cell growth, antibody titer, and product quality. *Biotechnol. Bioeng.* **2021,** *118* (11), 4305-4316.
33. Ben-David, U.; Siranosian, B.; Ha, G.; Tang, H.; Oren, Y.; Hinohara, K.; Strathdee, C. A.; Dempster, J.; Lyons, N. J.; Burns, R., et al., Genetic and transcriptional evolution alters cancer cell line drug response. *Nature* **2018,** *560* (7718), 325-330.
34. Kreutz, D.; Bileck, A.; Plessl, K.; Wolrab, D.; Groessl, M.; Keppler, B. K.; Meier, S. M.; Gerner, C., Response profiling using shotgun proteomics enables global metallodrug mechanisms of action to be established. *Chem. Eur. J.* **2017,** *23* (8), 1881-1890.
35. Meier-Menches, S. M.; Neuditschko, B.; Janker, L.; Gerner, M. C.; Schmetterer, K. G.; Reichle, A.; Gerner, C., A proteomic platform enables to test for AML normalization in vitro. *Front. Chem.* **2022,** *10*, 826346.
36. Paulitschke, V.; Eichhoff, O.; Cheng, P. F.; Levesque, M. P.; Höller, C., Proteomics approaches to understanding mitogen-activated protein kinase inhibitor resistance in melanoma. *Curr. Opin. Oncol.* **2016,** *28* (2), 172-179.
37. Gonzalez, D. M.; Medici, D., Signaling mechanisms of the epithelial-mesenchymal transition. *Sci. Signal.* **2014,** *7* (344), re8.
38. de Thé, H., Differentiation therapy revisited. *Nat. Rev. Cancer* **2017,** *18* (2), 117-127.
39. Burnett, A. K.; Russell, N. H.; Hills, R. K.; Bowen, D.; Kell, J.; Knapper, S.; Morgan, Y. G.; Lok, J.; Grech, A.; Jones, G., et al., Arsenic trioxide and all-trans retinoic acid treatment for acute promyelocytic leukaemia in all risk groups (AML17): results of a randomised, controlled, phase 3 trial. *Lancet Oncol.* **2015,** *16* (13), 1295-1305.
40. Freshney, R. I., *Culture of animal cells: A manual of basic technique and specialized applications*. 6th edition; John Wiley & Sons, Inc.: Hoboken, New Jersey, 2010.
41. Yokokura, S.; Kanaji, N.; Tadokoro, A.; Yokokura, S.; Kadowaki, N.; Bandoh, S., Confluence-dependent resistance to cisplatin in lung cancer cells is regulated by transforming growth factor-beta. *Exp. Lung Res.* **2016,** *42* (4), 175-181.
42. Garrido, C.; Ottavi, P.; Fromentin, A.; Hammann, A.; Arrigo, A. P.; Chauffert, B.; Mehlen, P., HSP27 as a mediator of confluence-dependent resistance to cell death induced by anticancer drugs. *Cancer Res.* **1997,** *57* (13), 2661-2667.
43. Neuditschko, B.; Leibetseder, M.; Brunmair, J.; Hagn, G.; Skos, L.; Gerner, M. C.; Meier-Menches, S. M.; Yotova, I.; Gerner, C., Epithelial cell line derived from endometriotic lesion mimics macrophage nervous mechanism of pain generation on proteome and metabolome levels. *Biomolecules* **2021,** *11* (8), 1230.
44. Fahy, E.; Sud, M.; Cotter, D.; Subramaniam, S., LIPID MAPS online tools for lipid research. *Nucleic Acids Res.* **2007,** *35*, W606-W612.
45. *RSTudio Team. RStudio: Integrated Development for R*, 2020, http://www.rstudio.com/.
46. Leitner, G. C.; Hagn, G.; Niederstaetter, L.; Bileck, A.; Plessl-Walder, K.; Horvath, M.; Kolovratova, V.; Tanzmann, A.; Tolios, A.; Rabitsch, W., et al., INTERCEPT pathogen reduction in platelet concentrates, in contrast to gamma irradiation, induces the formation of trans-arachidonic acids and affects eicosanoid release during storage. *Biomolecules* **2022,** *12* (9), 1258.
47. Lazar, C.; Burger, T. *imputeLCMD: A collection of methods for left-censored missing data imputation.* , version 2.1.; 2022, CRAN.R-project.org/package=imputeLCMD.
48. Wickham, H. *ggplot2: Elegant graphics for data analysis*, version 3.4.0.; 2016, ggplot2.tidyverse.org.
49. Weiss, T.; Taschner-Mandl, S.; Janker, L.; Bileck, A.; Rifatbegovic, F.; Kromp, F.; Sorger, H.; Kauer, M. O.; Frech, C.; Windhager, R., et al., Schwann cell plasticity regulates neuroblastic tumor cell differentiation via epidermal growth factor-like protein 8. *Nat. Commun.* **2021,** *12* (1), 1624.
50. Humphrey, S. J.; Karayel, O.; James, D. E.; Mann, M., High-throughput and high-sensitivity phosphoproteomics with the EasyPhos platform. *Nat. Protoc.* **2018,** *13* (9), 1897-1916.
51. Cox, J.; Mann, M., MaxQuant enables high peptide identification rates, individualized p.p.b.-range mass accuracies and proteome-wide protein quantification. *Nat. Biotechnol.* **2008,** *26* (12), 1367-1372.
52. Bateman, A.; Martin, M.-J.; Orchard, S.; Magrane, M.; Agivetova, R.; Ahmad, S.; Alpi, E.; Bowler-Barnett, E. H.; Britto, R.; Bursteinas, B., et al., UniProt: the universal protein knowledgebase in 2021. *Nucleic Acids Res.* **2021,** *49* (D1), D480-D489.
53. Kim, H. J.; Kim, T.; Xiao, D.; Yang, P., Protocol for the processing and downstream analysis of phosphoproteomic data with PhosR. *STAR Protoc.* **2021,** *2* (2), 100585.
54. Kim, H. J.; Kim, T.; Hoffman, N. J.; Xiao, D.; James, D. E.; Humphrey, S. J.; Yang, P., PhosR enables processing and functional analysis of phosphoproteomic data. *Cell Rep.* **2021,** *34* (8), 108771.
55. Ritchie, M. E.; Phipson, B.; Wu, D.; Hu, Y.; Law, C. W.; Shi, W.; Smyth, G. K., limma powers differential expression analyses for RNA-sequencing and microarray studies. *Nucleic Acids Res.* **2015,** *43* (7), e47-e47.
56. Wickham, H.; Francois, R.; Henry, L.; Müller, K. *dplyr: A grammar of data manipulation*, version 1.0.10.; 2022, dplyr.tidyverse.org.
57. Kassambara, A. *ggpubr: 'ggplot2' based publication ready plots*, R package version 0.4.0; 2020, CRAN.R-project.org/package=ggpubr.
58. Slowikowski, K. *ggrepel: Automatically position non-overlapping text labels with 'ggplot2'*, R package version 0.9.1; 2021, CRAN.R-project.org/package=ggrepel.
59. Chen, H.; Boutros, P. C., VennDiagram: a package for the generation of highly-customizable Venn and Euler diagrams in R. *BMC Bioinform.* **2011,** *12* (1), 35.

60. Balci, H.; Siper, M. C.; Saleh, N.; Safarli, I.; Roy, L.; Kilicarslan, M.; Ozaydin, R.; Mazein, A.; Auffray, C.; Babur, Ö., et al., Newt: a comprehensive web-based tool for viewing, constructing and analyzing biological maps. *Bioinformatics* **2021,** *37* (10), 1475-1477.
61. Perez-Riverol, Y.; Csordas, A.; Bai, J.; Bernal-Llinares, M.; Hewapathirana, S.; Kundu, D. J.; Inuganti, A.; Griss, J.; Mayer, G.; Eisenacher, M., et al., The PRIDE database and related tools and resources in 2019: improving support for quantification data. *Nucleic Acids Res.* **2019,** *47* (D1), D442-D450.
62. Zheng, P.-Z.; Wang, K.-K.; Zhang, Q.-Y.; Huang, Q.-H.; Du, Y.-Z.; Zhang, Q.-H.; Xiao, D.-K.; Shen, S.-H.; Imbeaud, S.; Eveno, E., et al., Systems analysis of transcriptome and proteome in retinoic acid/arsenic trioxide-induced cell differentiation/apoptosis of promyelocytic leukemia. *Proc. Natl. Acad. Sci.* **2005,** *102* (21), 7653-7658.
63. Miller, W. H., Jr.; Schipper, H. M.; Lee, J. S.; Singer, J.; Waxman, S., Mechanisms of action of arsenic trioxide. *Cancer Res.* **2002,** *62* (14), 3893-3903.
64. Dennis, E. A.; Norris, P. C., Eicosanoid storm in infection and inflammation. *Nat. Rev. Immunol.* **2015,** *15* (8), 511-523.
65. Shishehbor, M. H.; Zhang, R.; Medina, H.; Brennan, M. L.; Brennan, D. M.; Ellis, S. G.; Topol, E. J.; Hazen, S. L., Systemic elevations of free radical oxidation products of arachidonic acid are associated with angiographic evidence of coronary artery disease. *Free Radic. Biol. Med.* **2006,** *41* (11), 1678-1683.
66. Yu, G.; Zeng, X.; Wang, H.; Hou, Q.; Tan, C.; Xu, Q.; Wang, H., 14,15-Epoxyeicosatrienoic acid suppresses cigarette smoke extract-induced apoptosis in lung epithelial cells by inhibiting endoplasmic reticulum stress. *Cell. Physiol. Biochem.* **2015,** *36* (2), 474-486.
67. Wilks, A.; Black, S. M.; Miller, W. L.; Ortiz de Montellano, P. R., Expression and characterization of truncated human heme oxygenase (hHO-1) and a fusion protein of hHO-1 with human cytochrome P450 reductase. *Biochemistry* **2002,** *34* (13), 4421-4427.
68. Lightning, L. K.; Huang, H.-w.; Moënne-Loccoz, P.; Loehr, T. M.; Schuller, D. J.; Poulos, T. L.; de Montellano, P. R. O., Disruption of an active site hydrogen bond converts human heme oxygenase-1 into a peroxidase. *J. Biol. Chem.* **2001,** *276* (14), 10612-10619.
69. Petrache, I.; Otterbein, L. E.; Alam, J.; Wiegand, G. W.; Choi, A. M. K., Heme oxygenase-1 inhibits TNF-α-induced apoptosis in cultured fibroblasts. *Am. J. Physiol. Lung Cell Mol.* **2000,** *278* (2), L312-L319.
70. Jin, Z.; Gao, F.; Flagg, T.; Deng, X., Tobacco-specific nitrosamine 4-(methylnitrosamino)-1-(3-pyridyl)-1-butanone promotes functional cooperation of Bcl2 and c-Myc through phosphorylation in regulating cell survival and proliferation. *J. Biol. Chem.* **2004,** *279* (38), 40209-40219.
71. Andrew, A. S.; Mason, R. A.; Memoli, V.; Duell, E. J., Arsenic activates EGFR pathway signaling in the lung. *Toxicol. Sci.* **2009,** *109* (2), 350-357.
72. Sharma, M.; Sharma, S.; Arora, M.; Kaul, D., Regulation of cellular Cyclin D1 gene by arsenic is mediated through miR-2909. *Gene* **2013,** *522* (1), 60-64.
73. Chou, W.-C.; Hawkins, A. L.; Barrett, J. F.; Griffin, C. A.; Dang, C. V., Arsenic inhibition of telomerase transcription leads to genetic instability. *J. Clin. Invest.* **2001,** *108* (10), 1541-1547.
74. Loh, X.-Y.; Sun, Q.-Y.; Ding, L.-W.; Mayakonda, A.; Venkatachalam, N.; Yeo, M.-S.; Silva, T. C.; Xiao, J.-F.; Doan, N. B.; Said, J. W., et al., RNA-binding protein ZFP36L1 suppresses hypoxia and cell-cycle signaling. *Cancer Res.* **2020,** *80* (2), 219-233.
75. Zhao, C. Q.; Young, M. R.; Diwan, B. A.; Coogan, T. P.; Waalkes, M. P., Association of arsenic-induced malignant transformation with DNA hypomethylation and aberrant gene expression. *Proc. Natl. Acad. Sci.* **1997,** *94* (20), 10907-10912.
76. Bower, J. J.; Leonard, S. S.; Chen, F.; Shi, X., As(III) transcriptionally activates the gadd45a gene via the formation of H2O2. *Free Radic. Biol. Med.* **2006,** *41* (2), 285-294.
77. Tong, D.; Ortega, J.; Kim, C.; Huang, J.; Gu, L.; Li, G.-M., Arsenic inhibits DNA mismatch repair by promoting EGFR expression and PCNA phosphorylation. *J. Biol. Chem.* **2015,** *290* (23), 14536-14541.
78. Nardai, G.; Sass, B.; Eber, J.; Orosz, G.; Csermely, P., Reactive cysteines of the 90-kDa heat shock protein, Hsp90. *Arch. Biochem. Biophys.* **2000,** *384* (1), 59-67.
79. Hu, X.; Li, H.; Ip, T. K.-Y.; Cheung, Y. F.; Koohi-Moghadam, M.; Wang, H.; Yang, X.; Tritton, D. N.; Wang, Y.; Wang, Y., et al., Arsenic trioxide targets Hsp60, triggering degradation of p53 and survivin. *Chem. Sci.* **2021,** *12* (32), 10893-10900.
80. Stein, S.; Thomas, E. K.; Herzog, B.; Westfall, M. D.; Rocheleau, J. V.; Jackson, R. S.; Wang, M.; Liang, P., NDRG1 Is Necessary for p53-dependent Apoptosis. *J. Biol. Chem.* **2004,** *279* (47), 48930-48940.
81. Kim, E. H.; Yoon, M. J.; Kim, S. U.; Kwon, T. K.; Sohn, S.; Choi, K. S., Arsenic trioxide sensitizes human glioma cells, but not normal astrocytes, to TRAIL-induced apoptosis via CCAAT/enhancer-binding protein homologous protein-dependent DR5 up-regulation. *Cancer Res.* **2008,** *68* (1), 266-275.
82. Strum, S. W.; Gyenis, L.; Litchfield, D. W., CSNK2 in cancer: pathophysiology and translational applications. *Br. J. Cancer* **2021,** *126* (7), 994-1003.
83. Dawood, M.; Hamdoun, S.; Efferth, T., Multifactorial modes of action of arsenic trioxide in cancer cells as analyzed by classical and network pharmacology. *Front. Pharmacol.* **2018,** *9*, 143.
84. Muenyi, C.; Ljungman, M.; States, J., Arsenic disruption of DNA damage responses—Potential role in carcinogenesis and chemotherapy. *Biomolecules* **2015,** *5* (4), 2184-2193.
85. Giacinti, C.; Giordano, A., RB and cell cycle progression. *Oncogene* **2006,** *25* (38), 5220-5227.
86. Hu, Y.; Jin, X.; Snow, E. T., Effect of arsenic on transcription factor AP-1 and NF-κB DNA binding activity and related gene expression. *Toxicol. Lett.* **2002,** *133* (1), 33-45.

87. Almutairy, B.; Fu, Y.; Bi, Z.; Zhang, W.; Wadgaonkar, P.; Qiu, Y.; Thakur, C.; Chen, F., Arsenic activates STAT3 signaling during the transformation of the human bronchial epithelial cells. *Toxicol. Appl. Pharmacol.* **2022,** *436*, 115884.
88. Kim, S. H.; Yoo, H. S.; Joo, M. K.; Kim, T.; Park, J.-J.; Lee, B. J.; Chun, H. J.; Lee, S. W.; Bak, Y.-T., Arsenic trioxide attenuates STAT-3 activity and epithelial-mesenchymal transition through induction of SHP-1 in gastric cancer cells. *BMC Cancer* **2018,** *18* (1), 150.
89. Graw, S.; Chappell, K.; Washam, C. L.; Gies, A.; Bird, J.; Robeson, M. S.; Byrum, S. D., Multi-omics data integration considerations and study design for biological systems and disease. *Mol. Omics* **2021,** *17* (2), 170-185.
90. Paulitschke, P.; Keber, F.; Lebedev, A.; Stephan, J.; Lorenz, H.; Hasselmann, S.; Heinrich, D.; Weig, E. M., Ultraflexible nanowire array for label- and distortion-free cellular force tracking. *Nano Lett.* **2018,** *19* (4), 2207-2214.
91. Tyanova, S.; Temu, T.; Sinitcyn, P.; Carlson, A.; Hein, M. Y.; Geiger, T.; Mann, M.; Cox, J., The Perseus computational platform for comprehensive analysis of (prote)omics data. *Nat. Methods.* **2016,** *13* (9), 731-740.
92. Lo-Coco, F.; Avvisati, G.; Vignetti, M.; Thiede, C.; Orlando, S. M.; Iacobelli, S.; Ferrara, F.; Fazi, P.; Cicconi, L.; Di Bona, E., et al., Retinoic acid and arsenic trioxide for acute promyelocytic leukemia. *New Eng. J. Med.* **2013,** *369* (2), 111-121.
93. Sears, R. C., The Life Cycle of C-Myc: From Synthesis to Degradation. *Cell Cycle* **2014,** *3* (9), 1131-1135.
94. Ewens, K. G.; Bhatti, T. R.; Moran, K. A.; Richards-Yutz, J.; Shields, C. L.; Eagle, R. C.; Ganguly, A., Phosphorylation of pRb: mechanism for RB pathway inactivation in MYCN-amplified retinoblastoma. *Cancer Med.* **2017,** *6* (3), 619-630.
95. Liu, Q.; Zhang, H.; Smeester, L.; Zou, F.; Kesic, M.; Jaspers, I.; Pi, J.; Fry, R. C., The NRF2-mediated oxidative stress response pathway is associated with tumor cell resistance to arsenic trioxide across the NCI-60 panel. *BMC Med. Genomics* **2010,** *3* (1), 37.
96. Mohni, K. N.; Wessel, S. R.; Zhao, R.; Wojciechowski, A. C.; Luzwick, J. W.; Layden, H.; Eichman, B. F.; Thompson, P. S.; Mehta, K. P. M.; Cortez, D., HMCES maintains genome integrity by shielding abasic sites in single-strand DNA. *Cell* **2019,** *176* (1-2), 144-153 e113.

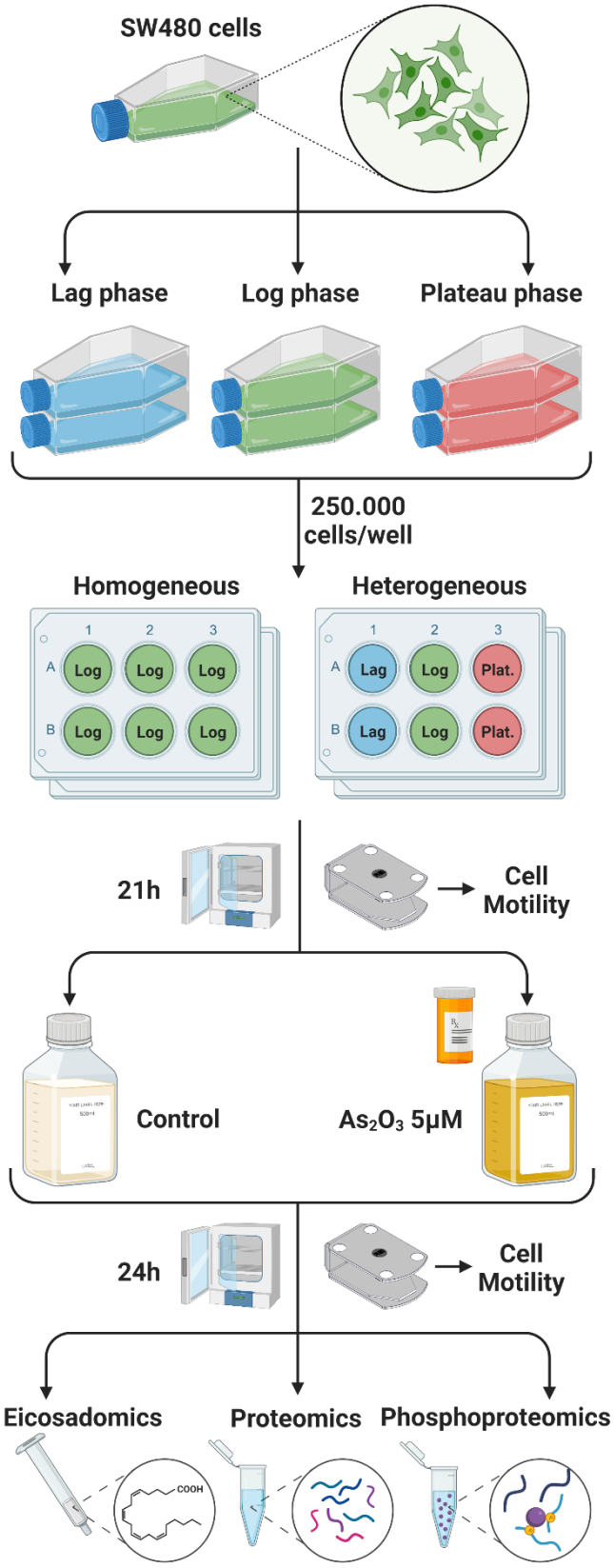

Figure 01. Experimental design to assess memory effects of subculture on multilevel omics readouts. SW480 colon carcinoma cells were cultured in complete medium. One culture was divided into three subcultures, each held at different phases of the growth curve. The first subculture was held

at Lag phase, the second subculture was held Log phase and the third subculture was held at plateau phase. Arsenic trioxide treatments (5 µM, 24 h) were performed using either homogeneous subculture (cells only from Log phase) or heterogeneous subculture (cells from all three subcultures). Controls and treatments were performed in hexuplicates with 250'000 cells per well. Cell growth and motility was continuously monitored using a PHIO Cellwatcher M. After 24 h incubation, the samples were worked up for multilevel omics analysis, including oxylipins and fatty acids from supernatants, as well as proteomics and phosphoproteomics from whole cell lysates.

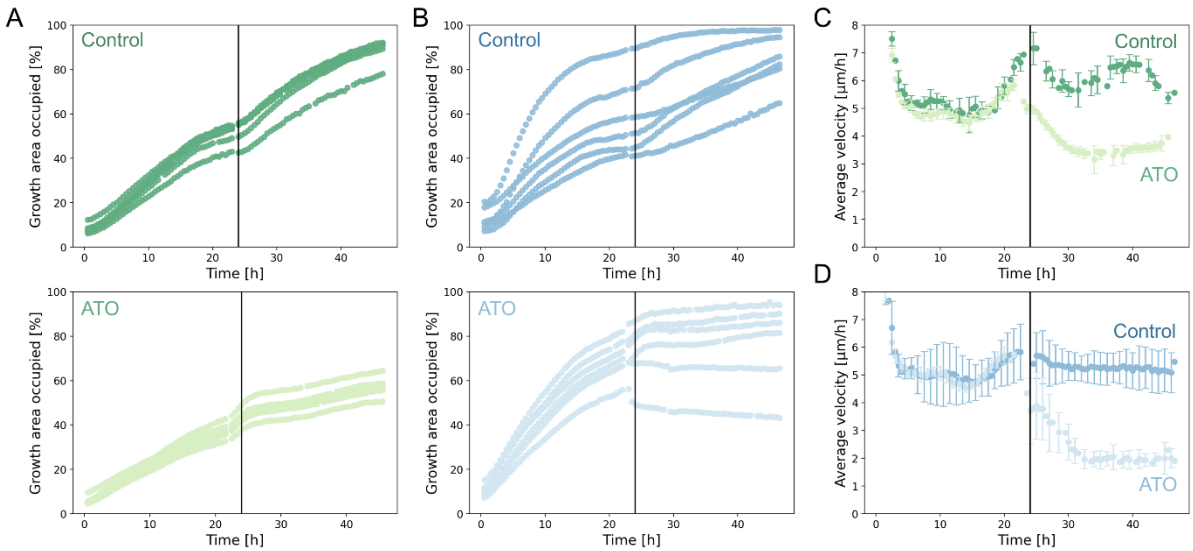

Figure 02. **Homogeneous subculture decreases variation of cell growth and motility compared to heterogeneous subculture.** Cell growth and motility was continuously monitored over the entire adhesion and treatment phases after subculture. Medium was replaced after 21 h either with containing vehicle control or arsenic trioxide (ATO, 5 µM) and incubated for further 24 h. The six individual wells were followed after homogenous subculture (**A**, green) and after heterogeneous subculture (**B**, blue). Treatment with to ATO reduced cell growth independently of subculture conditions (light green, light blue). Similarly, cell motility was reduced upon treatment with ATO independently of homogeneous (**C**, green) and heterogeneous (**D**, blue) subcultures, but variation increases in the latter.

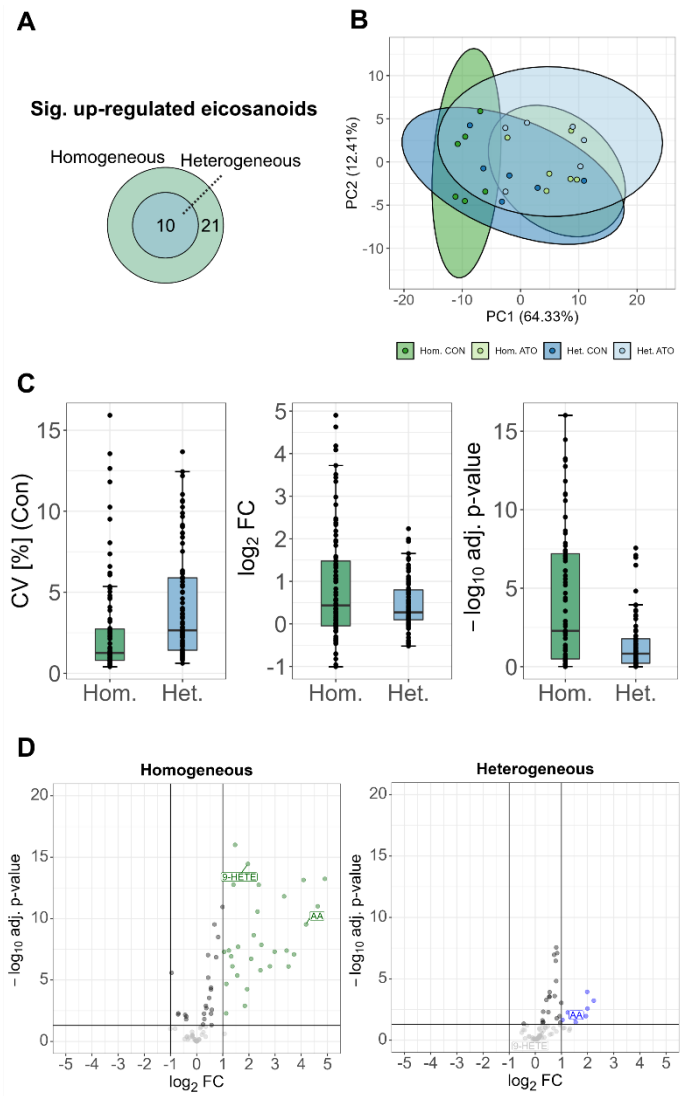

Figure 03. **Homogeneous subculture dcreases variation of oxylipin and fatty acid data compared to heterogeneous subculture.** (**A**) The Venn diagram illustrates the shared and specific upregulated eicosanoids upon treatment of SW480 cancer cells with arsenic trioxide (ATO). (**B**) Principal component analysis (PCA) of normalized area under the curve (nAUC)-intensity values of identified oxylipins and fatty acids in control and ATO-treated SW480 cells of the homogeneous (green) and heterogeneous (blue) subcultures. The first two principal components separate homogeneous controls from ATO-treatments, while this was not the observed for the heterogeneous subculture. Ellipses represent the 95% confidence intervals. (**C**) Boxplots of the control samples displaying the coefficients of variance (CV) of nAUC-intensities of oxylipins and fatty acids among six biological replicates in homogeneous (green) and heterogeneous (blue) subcultures. Also, the $\log_2$-fold-changes (FC) of the perturbation of nAUC-intensities was plotted as boxplots for homogeneous and heterogeneous subcultures, as well as the associated multiple testing corrected p-value. (**D**) Volcano plots showing the ATO-induced perturbation of the homogeneous (green) and heterogeneous (blue) subcultures on the oxylipin and fatty acid level. Multiple testing corrected significant regulations are coloured.

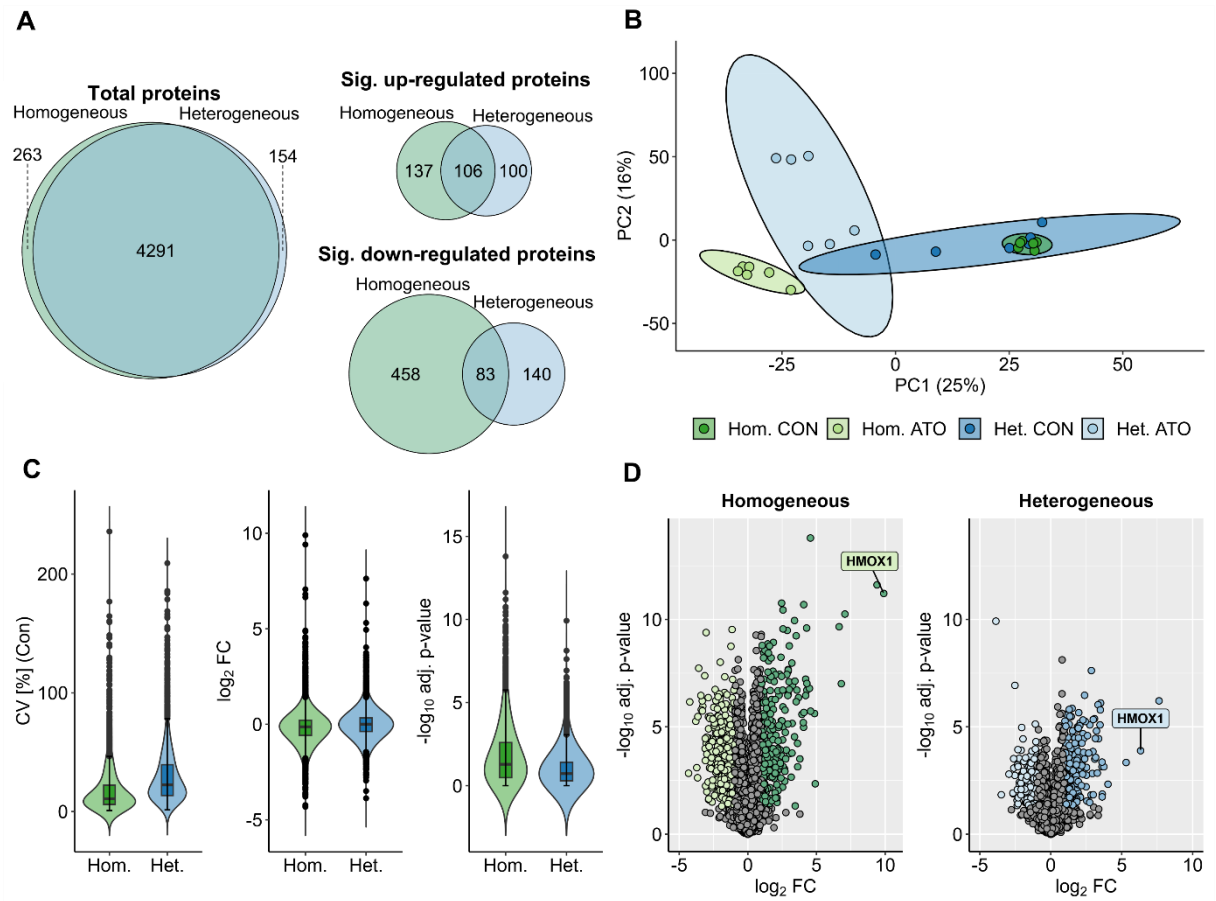

Figure 04. **Homogeneous subculture decreases variation of proteomics data compared to heterogeneous subculture.** (**A**) The Venn diagrams illustrate shared protein identifications upon treatment with arsenic trioxide (ATO) between the homogeneous and heterogeneous subcultures, as well as shared significantly up- and down-regulated proteins (adj. p-value ≤0.05, fold change ≥1 or ≤1). (**B**) Principal component analysis (PCA) of LFQ-intensity values of identified proteins in control and ATO-treated SW480 cells of the homogeneous (green) and heterogeneous (blue) subcultures. The first two principal components separate homogeneous controls from ATO-treatments, while this was not the observed for the heterogeneous subculture. Ellipses represent the 95% confidence intervals. (**C**) Violin plots of the control samples displaying the coefficients of variance (CV) of LFQ-intensities among six biological replicates in homogeneous (green) and heterogeneous (blue) subcultures. Also, the log_2-fold-changes (FC) of the perturbation of LFQ-intensities was plotted as violin plots for homogeneous and heterogeneous subcultures, as well as the associated multiple testing corrected p-value. (**D**) Volcano plots showing the global ATO-induced perturbation of the homogeneous (green) and heterogeneous (blue) subcultures on the protein level. Multiple testing corrected significant protein regulations are coloured.

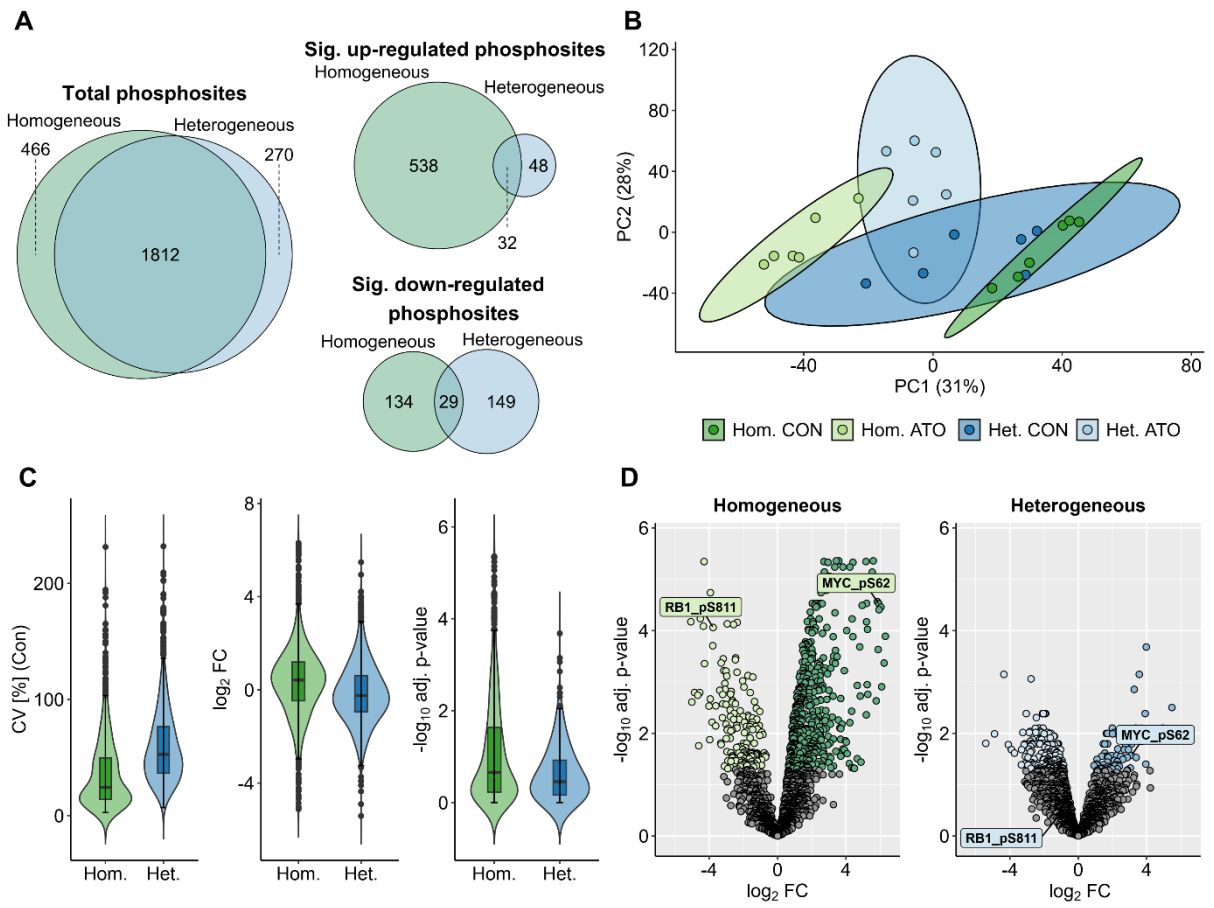

Figure 05. **Homogeneous subculture decreases variation of phosphoproteomic data compared to heterogeneous subculture.** (**A**) The Venn diagrams illustrate shared phosphosite identifications upon treatment with arsenic trioxide (ATO) between the homogeneous and heterogeneous subcultures, as well as shared significantly up- and downregulated phosphosites (adj. p-value ≤0.05, fold change ≥1 or ≤1). (**B**) Principal component analysis (PCA) of LFQ-intensity values of identified phosphosites in control and ATO-treated SW480 cells of the homogeneous (green) and heterogeneous (blue) subcultures. The first two principal components separate homogeneous controls from ATO-treatments, while this was not the observed for the heterogeneous subculture. Ellipses represent the 95% confidence intervals. (**C**) Violin plots of the control samples displaying the coefficients of variance (CV) of LFQ-intensities of phosphosites among six biological replicates in homogeneous (green) and heterogeneous (blue) subcultures. Also, the log_2-fold-changes (FC) of the perturbation of phosphosite LFQ-intensities was plotted as violin plots for homogeneous and heterogeneous subcultures, as well as the associated multiple testing corrected p-value. (**D**) Volcano plots showing the ATO-induced perturbation of the homogeneous (green) and heterogeneous (blue) subcultures on the phosphosite level. Multiple testing corrected significant protein regulations are coloured.

A

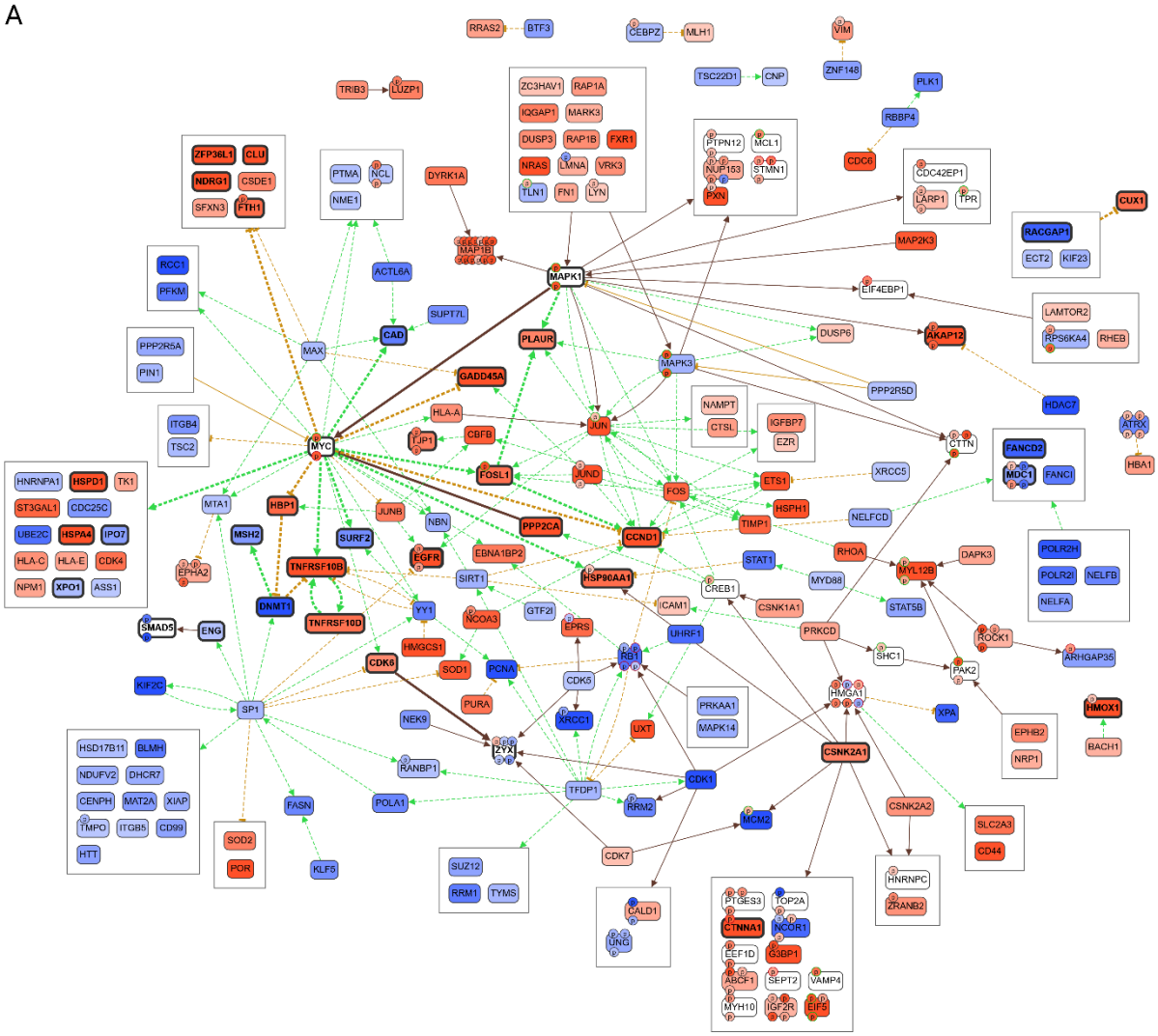

B

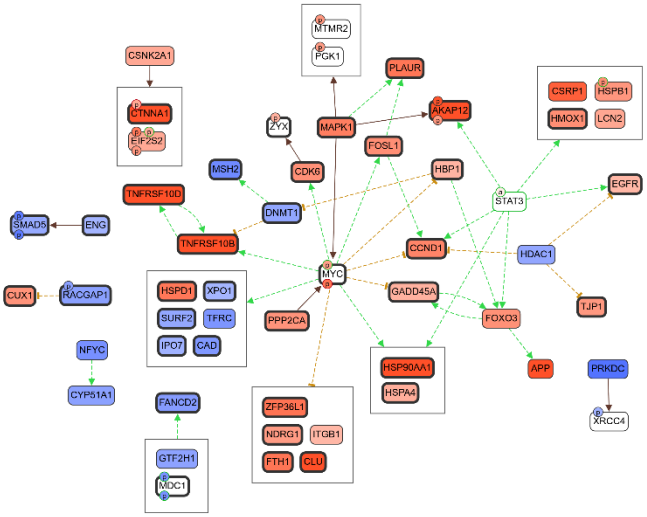

Figure 06. Bilevel CausalPath analysis using global proteomic and phosphoproteomic data of arsenic trioxide (ATO)-induced perturbation networks from homogeneous (**A**) and heterogeneous (**B**) subcultures. The homogeneous and heterogeneous subcultures yielded 321 and 58 causal conjectures, respectively. The memory effect of heterogeneous subculture increases experimental variation and

reduces the information content of the resulting perturbation network for the ATO-treatment on SW480 cancer cells. Red represents upregulated gene expression products or phosphorylation events. Blue represents down-regulated gene expression products or phosphorylation events. Dashed lines represent gene expression changes (green = positive correlation of expression, orange = negative correlation of expression. Continuous-line brown arrows represent phosphorylation events. Phosphosites may be activating (green frame) or inactivating (red frame). STAT3 was annotated ("a") by the CausalPath algorithm due to the concerted upregulation of gene expression products in the perturbation network of the heterogeneous subculture (**B**). Bold lines and boxes in (**A**) reflect those causal conjectures that were also identified in (**B**). *A high-resolution image of the perturbation network is provided as a supplementary figure.*